ADVANCES IN ATMOSPHERIC SCIENCES, VOL. 36, OCTOBER 2019, 1078–1088

• **Original Paper** •

Main Detrainment Height of Deep Convection Systems over the Tibetan Plateau and Its Southern Slope

Quanliang CHEN* , Guolu GAO , Yang LI , Hongke CAI , Xin ZHOU , and Zhenglin WANG

School of Atmospheric Sciences, Chengdu University of Information Technology and Plateau Atmosphere and Environment Key Laboratory of Sichuan Province, Chengdu 610225, *China*

(Received 11 January 2019; revised 29 March 2019; accepted 13 May 2019)

ABSTRACT

Deep convection systems (DCSs) can rapidly lift water vapor and other pollutants from the lower troposphere to the upper troposphere and lower stratosphere. The main detrainment height determines the level to which the air parcel is lifted. We analyzed the main detrainment height over the Tibetan Plateau and its southern slope based on the CloudSat Cloud Profiling Radar 2B_GEOPROF dataset and the Aura Microwave Limb Sounder Level 2 cloud ice product onboard the A-train constellation of Earth-observing satellites. It was found that the DCSs over the Tibetan Plateau and its southern slope have a higher main detrainment height (about 10–16 km) than other regions in the same latitude. The mean main detrainment heights are 12.9 and 13.3 km over the Tibetan Plateau and its southern slope, respectively. The cloud ice water path decreases by 16.8% after excluding the influences of DCSs, and the height with the maximum increase in cloud ice water content is located at 178 hPa (about 13 km). The main detrainment height and outflow horizontal range are higher and larger over the central and eastern Tibetan Plateau, the west of the southern slope, and the southeastern edge of the Tibetan Plateau than that over the northwestern Tibetan Plateau. The main detrainment height and outflow horizontal range are lower and broader at nighttime than during daytime.

Key words: main detrainment height, deep convection systems, Tibetan Plateau and its southern slope, A-train

Citation: Chen, Q. L., G. L. Gao, Y. Li, H. K. Cai, X. Zhou, and Z. L. Wang, 2019: Main detrainment height of deep convection systems over the Tibetan Plateau and its southern slope. *Adv. Atmos. Sci.*, **36**(10), 1078–1088, https://doi.org/10.1007/s00376-019-9003-3.

Article Highlights:

- The mean main detrainment heights are 12.9 and 13.3 km over the Tibetan Plateau and its southern slope, respectively.
- The cloud ice water path decreases by 16.8% after excluding the influences of DCSs over the Tibetan Plateau and its southern slope.

1. Introduction

Deep convection systems (DCSs) are a key link in exchanges between the stratosphere and troposphere (Holton et al., 1995; Sherwood and Dessler, 2000; Stohl et al., 2003; Jensen et al., 2007; Liu et al., 2007; Corti et al., 2008; Hong et al., 2008; Lü et al., 2009). As an important complement to the large-scale fluid dynamic suction pump process, DCSs can rapidly transport air parcels from the lower troposphere and boundary layer into the upper troposphere and lower stratosphere (UTLS) (Dessler and Sherwood, 2004; Mullendore et al., 2005; Fueglistaler et al., 2009; Liu et al., 2010) and detrain cloud into the upper troposphere (Raymond and Blyth, 1986; Sherwood and Dessler, 2003; Andreae et al., 2004). In same cases of overshooting convection, the cloud top of the DCSs can penetrate the tropopause, where the cloud mixes directly with the stratosphere through turbulent exchange and isentropic advection dispersion (Holton and Gettelman, 2001; Khaykin et al., 2009; Hassim and Lane, 2010; Livesey et al., 2013). This rapid process can change the distribution of chemical components in the UTLS, which, in turn, may affect the global climate via indirect radiation forcing (Danielsen, 1993; de F. Forster and Shine, 1999, 2002; Kirk-Davidoff et al., 1999; Luo and Rossow, 2004; Corti et al., 2005; Wright et al., 2009; Solomon et al., 2010, 2011).

Previous studies have pointed out that DCSs affect the atmospheric composition budget of the UTLS via two different steps (Sherwood, 2000; Dessler, 2002; Gettelman et al., 2002; Park et al., 2009). DCSs rapidly lift the air parcel into the main detrainment layer, and then the detrained air will be slowly dehydrated by atmospheric circulation and diabatic heating until

* Corresponding author: Quanliang CHEN
Email: chenql@cuit.edu.cn

it passes through the coldest point of the tropopause (Mote et al., 1996; Sherwood and Dessler, 2000). The freeze–dry function is weaker at higher detrainment heights but its effect on the atmospheric component of the stratosphere is stronger (Brewer, 1949; Jensen et al., 2001; Schiller et al., 2009). The position of the main detrainment height determines the height at which the substances in the lower troposphere and boundary layer can be rapidly transported by the DCSs. However, different DCSs have different outflow heights depending on the local ambient relative humidity, the vertical stability and depth of the thunderstorm cloud. Therefore, investigation of detrainment height location is very important.

Many studies have investigated the characteristics of DCSs (Zipser et al., 2006; Houze et al., 2007; Devasthale and Fueglistaler, 2010; Romatschke et al., 2010; Luo et al., 2011; Xu, 2013; Qie et al., 2014; Takahashi and Luo, 2014; Shi et al., 2017). However, these studies largely focused on the features of the core of DCSs, with their main detrainment height receiving little attention. The anvil, as a proxy of the main detrainment height, is located at the top of cumulus clouds around the level of neutral buoyancy (Stommel, 1947; Morton et al., 1956; Squires and Turner, 1962; Raymond and Blyth, 1986; de Rooy and Siebesma, 2008, 2010; Heus and Jonker, 2008). The Tibetan Plateau and its southern slope are important pathways for stratosphere–troposphere exchange (Zhou et al., 1995; Bannister et al., 2004; Gettelman et al., 2004; Li et al., 2005; Fu et al., 2006; Randel and Park, 2006; Park et al., 2007; Tian et al., 2008; Randel et al., 2010; Chen et al., 2012; Long et al., 2016; Sun et al., 2017). Thus, further investigation of the main detrainment height over the Tibetan Plateau and its southern slope will help us to estimate the contribution of DCSs to global stratosphere–troposphere exchange and quantify the atmospheric composition budget of the UTLS.

In this study, we used satellite data to investigate the main detrainment height over the Tibetan Plateau and its southern slope (Fig. 1). The paper is structured as follows: Section 2 introduces the A-train constellations, including the CloudSat Cloud Profiling Radar (CPR) and Aura Microwave Limb Sounder (MLS), the methods used to characterize the deep convective core (DCC) and anvil, and explains how we assessed the ice water content (IWC) of the background field of deep convection. Section 3 derives the main detrainment height over the Tibetan Plateau and its southern slope and analyzes the spatial and temporal features of the detrainment level. Section 4 compares these features with the change in the ambient field of the IWC and the ice water path (IWP) when the DCSs detrain air into the UTLS. Finally, our conclusions are presented in section 5.

2. Datasets and methods

2.1. *Datasets*

We used CloudSat and MLS data for June–August 2006–16, except for the year 2011 when a battery anomaly caused the CloudSat satellite to stop collecting data and to lose formation with the A-train. The datasets include 2B-GEOPROF_R04 (http://cloudsat.atmos.colostate.edu/data) and MLS-L2GP-IWC_v04 (https://daac.gsfc.nasa.gov/datasets/ML2IWC_V004). CloudSat, which forms part of the Afternoon Constellation or A-train of Earth-observing satellites, carries the CPR instrument, which has a high sensitivity toward smaller cloud droplets (Stephens et al., 2008). According to the CloudSat data, an accurate detrainment height and the anvil of DCSs can be obtained and detected. The CPR instrument can therefore directly observe the detrained anvil to obtain the main detrainment height. The Aura MLS, which follows about 15 minutes behind CloudSat, can detect changes in the atmospheric components when the detrainment caused by a DCS is recognized by the CPR (Livesey et al., 2006). Such dual observations are beneficial in obtaining a comprehensive view of the outflow process.

The A-train includes several Earth-observing satellites that follow the close orbital track within minutes of each other. They provide comprehensive information about a wide variety of climate parameters (Savtchenko et al., 2008; L'Ecuyer and Jiang, 2011). CloudSat launched on 28 April 2006. It successfully joined the A-train alignment on 1 June 2006 and exited

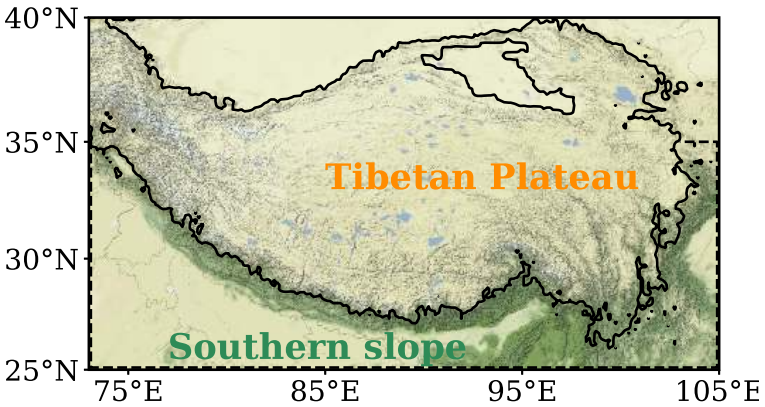

Fig. 1. Location of the Tibetan Plateau and its southern slope (25°–40°N, 73°–105°E). The area outlined by the black solid line is the Tibetan Plateau and the region to the south of 35°N with elevation < 3000 m is the southern slope. The topographic base map is from http://maps.stamen.com/.

the A-train on 26 February 2018. The CPR carried onboard the CloudSat platform was designed to have a strong cloud detection sensitivity for precipitation and cloud particles, with an along-track resolution of 1.9 km and a vertical resolution of 240 m (Stephens et al., 2002, 2008). The Aura satellite was successfully launched on 25 July 2004 and follows about 15 minutes behind CloudSat in the A-train satellite formation. The MLS instrument onboard the Aura satellite uses microwave emissions to measure trace amounts of gases, volcanic eruptions, cloud ice, temperature and geopotential height in the upper troposphere and stratosphere (Waters et al., 2006; Wu et al., 2008).

2.2. *Methods*

The radar echo from the backscattering of cloud and rain droplets can be used to recognize DCSs, including the DCC, stratiform precipitation and the anvil. The CloudSat CPR has been used to study deep convection (Chung et al., 2008; Iwasaki et al., 2010; Luo et al., 2011), overshooting (Luo et al., 2008; Bedka et al., 2012; Iwasaki et al., 2012; Takahashi and Luo, 2012), detrained anvils (Takahashi and Luo, 2012) and aerological cirrus clouds (Sassen et al., 2009). We detected DCSs over the Tibetan Plateau and its southern slope using the following methods.

We used a cloud mask of > 30 to obtain high-quality data (Mace, 2007). Radar echo data were used to detect the DCC and the cloud-top height of the DCC (DCC_CTH) required to ensure that the DCS could lift an air parcel to > 14 km, the height at which the UTLS is affected (Highwood and Hoskins, 1998; Folkins et al., 1999). The distance between the cloud base and the surface was < 3 km and the maximum echo value was > 10 dB*Z* to exclude clouds from non-DCSs. We looked for the detrained anvil near the DCC. The anvil should be a 4–5 km thick heterogeneous layer (Cetrone and Houze, 2009; Yuan and Houze, 2010; Yuan et al., 2011) and the cloud base height of the anvil (anvil_CBH) should be > 9 km to preclude radar echoes from stratiform precipitation. The height of maximum echo inside the anvil is the height of the maximum mass detrainment (anvil_maxMass), which means that the largest amount of air is detrained in this layer (Takahashi and Luo, 2012). We obtained data for 1241 DCSs over a 10-year period. A total of 669 DCSs showed clear detrainment, which requires a horizontal scale of the anvil > 20 km (see Fig. 2).

The Aura satellite follows CloudSat on an adjacent track. The Aura MLS measures the change in the ambient IWC after the CloudSat CPR has probed the DCSs. The IWC detrained by the DCSs has a short life cycle of about 1–2 days (Luo and Rossow, 2004). The distribution of the IWC is more directly affected by the DCS than other gaseous pollutants (e.g., CO, HCN, CH_3Cl and chlorofluorocarbons) with a longer life cycle.

3. Characteristics of the main detrainment height of DCSs

The frequency distribution of the variation in the reflectivity with height provides more insights into the structure of the anvil cloud and the outflow processes during deep convection (Steiner et al., 1995; Cetrone and Houze, 2009). Figure 3 shows the frequency distribution of the reflectivity with the height of anvil over the Tibetan Plateau and its southern slope. The anvil heights of DCSs are located at the altitude of about 10–16 km over the Tibetan Plateau and its southern slope. Most anvil heights of DCSs are located at 13–14 km. This is consistent with Park et al. (2008), who reported that the strongest outflow height over the South Asia–Tibetan Plateau area is 13–15 km, based on the position of pollutants in the anticyclone. Most of the anvil radar echoes are concentrated at about −20 dBZ, which means that small cloud and ice particles account for the main part of the anvil's detrainment. The small ice-phase particles produce a strong influence because the

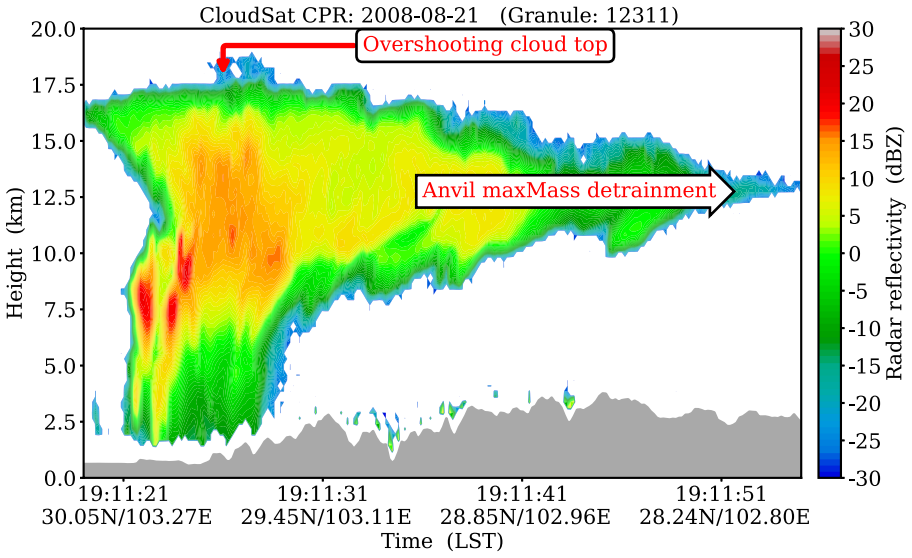

Fig. 2. An example of a DCS that generated on 21 August 2008. The gray shadow represents the topography, and the red lettering annotates the cloud top of the DCC and the anvil maximum mass detrainment.

small particles affected by the weak gravitational force have a slow falling speed, which makes it easy for the ice-phase particles to rest on the detrainment height and further transport into the upper troposphere and lower stratosphere via the vertical and horizontal current (Folkins et al., 1999; Alcala and Dessler, 2002).

Figure 3 shows that the main detrainment height over the Tibetan Plateau region and its southern slope is higher than that over tropical and global deep convection. Folkins and Martin (2005) concluded 12 km to be the main height of deep convective outflow in the tropics, according to a one-dimensional model of the tropics constrained by observed mean temperature and water vapor profiles. Takahashi and Luo (2012) used the CloudSat datasets to calculate the global mean outflow height as 10.7 km; the pixel samples were limited by an echo top height of 10 dBZ > 10 km. The higher outflow height over the Tibetan Plateau and its southern slope favors more water vapor and aerosols detrained by deep convection to be transported into the stratosphere. As a result, less mass is lost during upward movement.

The detrainment caused by deep convection over the Tibetan Plateau region and its southern slope is different as a result of the complex topography and atmospheric circulation. Figure 4 shows the outflow height/horizontal range of deep convections over the Tibetan Plateau region. It is apparent that the maximum mass outflow height/outflow horizontal range of DCSs is higher/larger over the central and eastern Tibetan Plateau, the west of the southern slope, and the southeastern edge of the Tibetan Plateau than that over the northwestern Tibetan Plateau. The proportion of DCSs with outflow height between 12.5 and 13.5 km is 53.66%, while below 11.5 km it is only 2.84%. About 72.35% of the DCSs have outflow horizontal ranges < 100 km. The mean outflow height over the Tibetan Plateau and its southern slope is 12.9 and 13.3 km, respectively, i.e., the mean outflow height over the southern slope is higher than that over the Tibetan Plateau. The thermodynamic function of the surface determines the population distribution of DCSs; the air parcels of the planetary boundary layer over the southern slope have a higher equivalent potential temperature than over the Tibetan Plateau, thus inducing deeper and more intense convective systems to be generated at the southern slope (Luo et al., 2011; Xu, 2013; Qie et al., 2014; Wu et al., 2016). In addition, the nocturnal moist low-level jet compensating the instability is also a crucial factor in the triggering of deep convection over the southern slope (Houze et al., 2007; Romatschke et al., 2010). It is possible that the intense deep convection over the southern slope produces a higher detrainment height than that over the Tibetan Plateau. Wu et al. (2004) determined that the intense surface radiation heating over the Tibetan Plateau results in low pressure at low levels and high pressure at middle and upper levels, which induces updrafts in the east of the Tibetan Plateau and downdrafts in the west. This phenomenon also explains why deeper and wider convective systems occur over the central and eastern Tibetan Plateau.

The CloudSat CPR satellite passes the equator at about 1330 LST (daytime; LST = UTC+6) and 0130 LST (nighttime). Figure 5 shows the distribution of outflow height and outflow horizontal range of DCSs during daytime and at nighttime. It is apparent that the DCSs with outflow heights of < 13 km and outflow horizontal ranges of > 100 km are more frequent at nighttime than during daytime, i.e., nocturnal deep convections detrain at relatively low heights but influence a wider area. According to traditional parcel theory, during the daytime, solar radiation heats the surface and produces more convective available potential energy and a higher level of neutral buoyancy, which favors convective development in the vertical direction (Mapes, 1993; Kingsmill and Houze, 1999). At nighttime, however, the lower temperatures and energy make it difficult for convection to reach a higher outflow height, meaning the cloud is more likely to detrain in a horizontal direction.

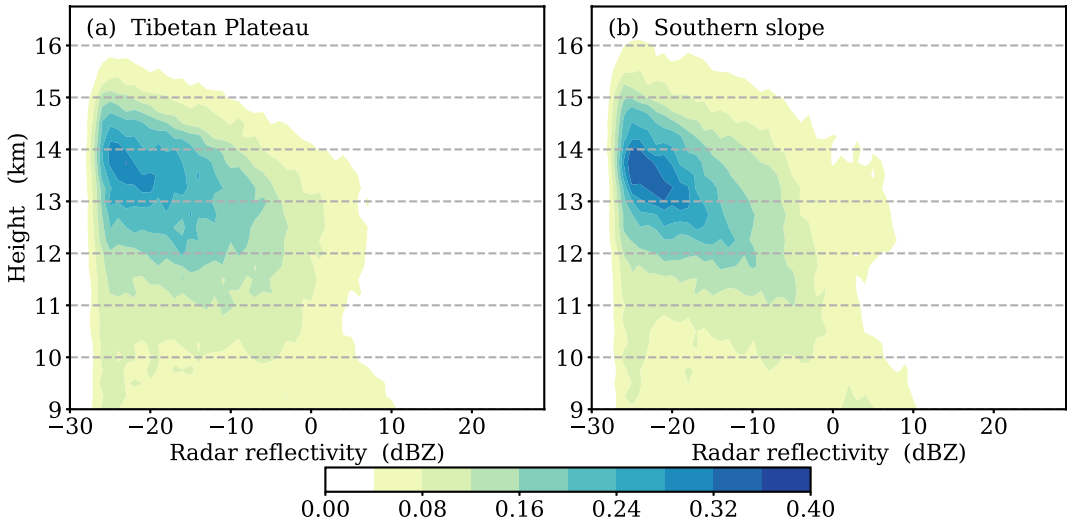

Fig. 3. Contour map of the frequency distribution of the reflectivity with the anvil height over (a) the Tibetan Plateau and (b) its southern slope. The reflectivity is from CloudSat CPR data. The contours show the bin counts divided by the total counts. Bin dimensions: 1 dBZ × 250 m.

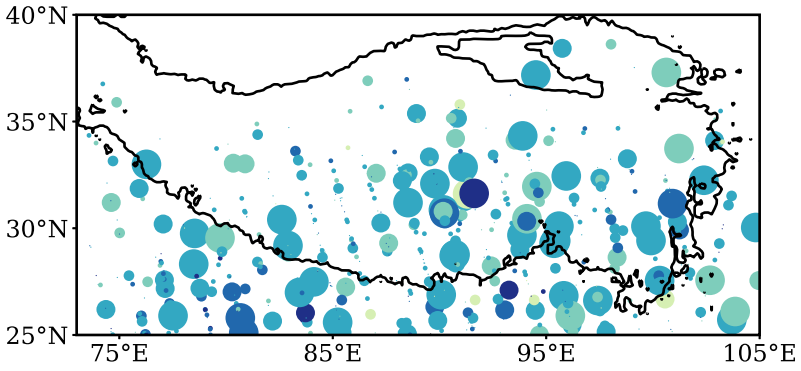

	⩽ 11.5 km	11.5-12.5 km	12.5-13.5 km	13.5-14.5 km	⩾ 14.5 km	Sum
⩽ 50 km	1.64%	8.07%	19.13%	8.67%	2.99%	40.51%
50-100 km	0.30%	5.23%	18.54%	5.98%	1.79%	31.84%
100-150 km	0.60%	2.99%	7.03%	2.24%	0.15%	13.00%
150-200 km	0.15%	2.09%	4.33%	1.05%	0.30%	7.92%
⩾ 200 km	0.15%	1.20%	4.63%	0.60%	0.15%	6.73%
Sum	2.84%	19.58%	53.66%	18.54%	5.38%	100.00%

Fig. 4. Top: Spatial distribution of outflow horizontal range and maximum mass outflow height of DCSs. Bottom: Frequency of different outflow heights/horizontal ranges of DCSs. The depth of the dot color and the size of the dot represent how high the maximum mass outflow height is and how wide the outflow horizontal range is, respectively.

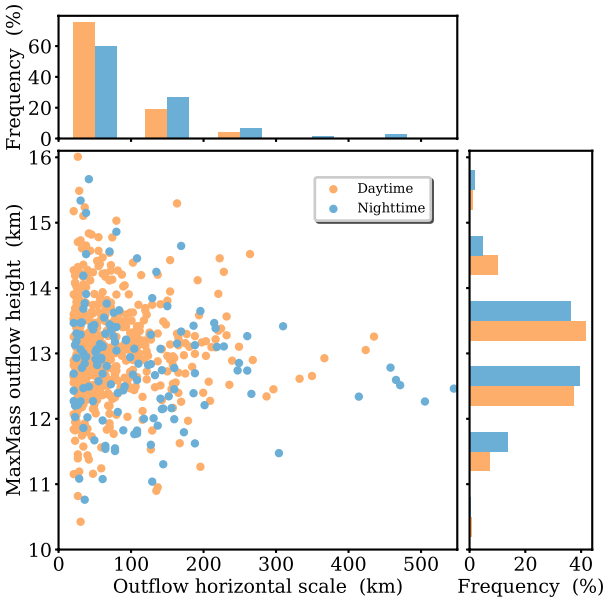

Fig. 5. Distribution of outflow height and outflow horizontal range of DCSs in the daytime (orange dots, 1200–1330 LST) and at nighttime (blue dots, 0000–0130 LST). The histograms show the probability density function of the dots.

4. Effect of the main detrainment height variations on cloud IWC

When cloud detrains an air parcel and mixes it with the ambient air, the cloud IWC increases rapidly. IWC data from the Aura MLS were used to investigate the effect of main detrainment height variations on the cloud IWC. Here, we define two events: DCS events and non-DCS events. A DCS event is one in which the ambient IWC observed by MLS is directly influenced by the DCS observed by CloudSat. In contrast, a non-DCS event describes the ambient IWC when the anterior CloudSat did not observe the DCS.

Besides the detection of radar echoes, a sharp increase in ambient IWC could directly prove the detrainment height of deep convection. Figure 6 shows the mean profiles of the cloud IWC over the Tibetan Plateau and its southern slope during the DCS events and non-DCS events and the differences between the profiles. An extreme value is located at 178 hPa (height of about 13 km), which coincides with the main detrainment height of DCSs directed by the radar echoes. The profiles of radar echoes and atmospheric components highlight the detrainment height of deep convection at about 178 hPa or 13 km. In the DCS scenario, the mean profile of IWC over the southern slope is higher than that over the Tibetan Plateau, since the deeper and wider convection is located at the southern slope, as mentioned above. In another insight, the magnitude of the increase in IWC over the southern slope is less than that over the Tibetan Plateau (Fig. 6b). The results of the significance testing also show that the deep convection over the Tibetan Plateau has a more obvious hydrating effect for the lower stratosphere. Over the Tibetan Plateau, the differences between profiles during DCS events and during non-DCS events from 215 to 83 hPa are signi-

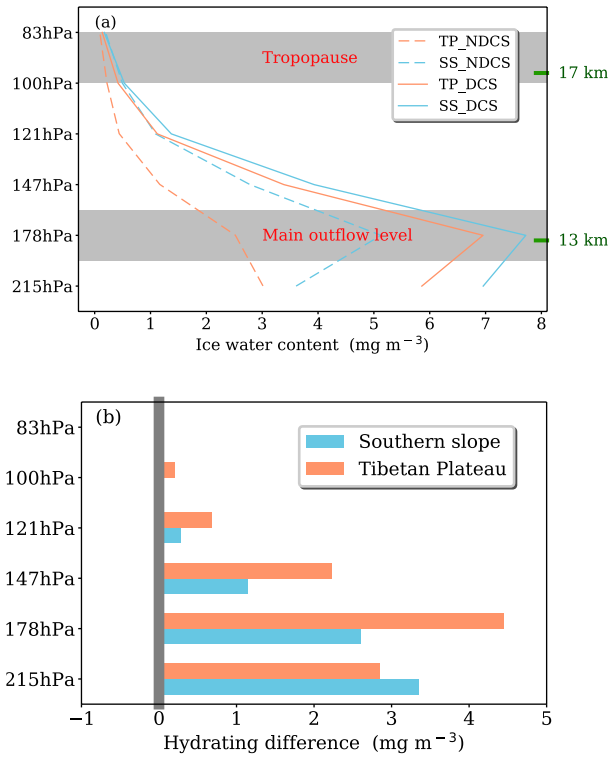

Fig. 6. (a) Mean profiles of cloud IWC over the Tibetan Plateau and its southern slope during DCS events and non-DCS events. Dashed lines and solid lines represent non-DCS and DCS events, respectively. (b) Differences between profiles during DCS events and non-DCS events.

ficant at the 95% confidence level. On the southern slope, the differences lower than 100 hPa are significant.

Deep convection has an important influence for the horizontal distribution of water vapor in the upper troposphere and lower stratosphere (Mullendore et al., 2005). Figures 7 and 8 show the distributions of the IWC at 178 hPa and 121 hPa over the Tibetan Plateau region, respectively, during the DCS events and non-DCS events. The area with more IWC coincides with the distribution of DCSs shown in Fig. 4, which means that the increase in IWC is closely related to the detrainment of deep convection at near real-time. The differences in IWC between the DCS and non-DCS events over the central and eastern areas of the Tibetan Plateau, the western area of the southern slope, and the southeastern edge of the Tibetan Plateau are significant at the 95% confidence level. The clearest evidence of the main detrainment height is seen at 178 hPa. It is noteworthy that the non-DCS scenario does not mean that the atmospheric environment is one of a clear sky. Cirrus cloud is included in the non-DCS scenario. Therefore, the IWC in the upper troposphere is higher than that in the clear-sky condition (Fig. 7a).

These horizontal and vertical results prove that the impact of deep convection for IWC is significant at near real-time. Nevertheless, since the frequency of deep convection is low, the effect of the long periodicity of deep convection detrainment remains uncertain. We estimate the contribution of deep convection to the summer mean IWP field by comparing the differ-

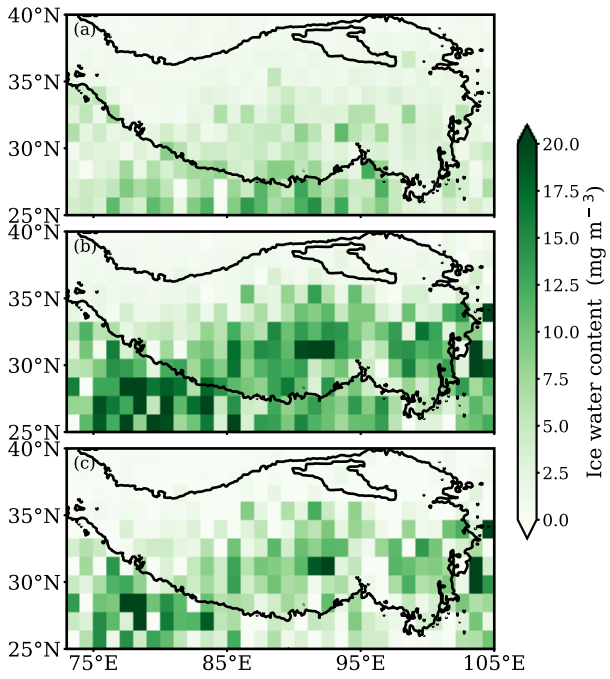

Fig. 7. Distributions of IWC at 178 hPa during (a) non-DCS events and (b) DCS events, and (c) the differences between (b) and (a).

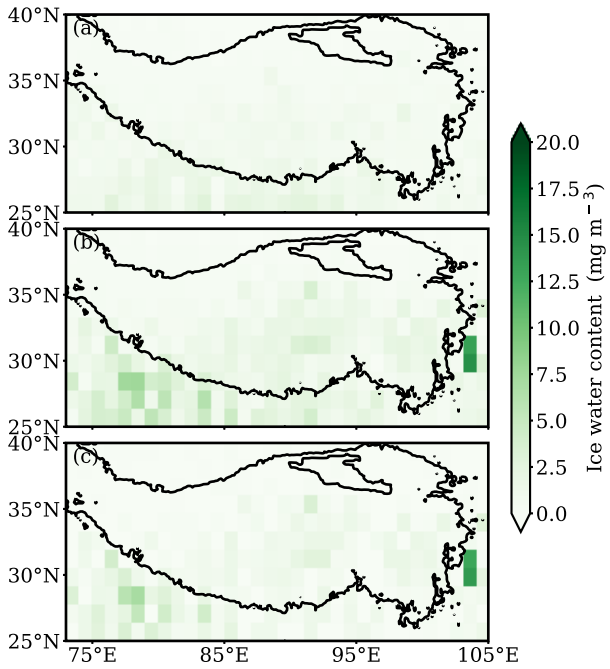

Fig. 8. As in Fig. 7 but at 121 hPa.

ence in mean IWP between all samples from the MLS detector and selected samples after eliminating DCS events. Figure 9 shows the distribution of the IWP (column total of IWC above 6 km) for all IWP samples (including DCS and non-DCS events) and for non-DCS events in June, July and August. After removing the influence of DCSs, the IWP decreases by ~2.83 g m^{-2} on average (reduction of 16.8%). In the area where DCSs occur frequently, the maximum reduction can be as much as 23.82 g m^{-2}. Figure 10 shows the latitudinal and meridi-

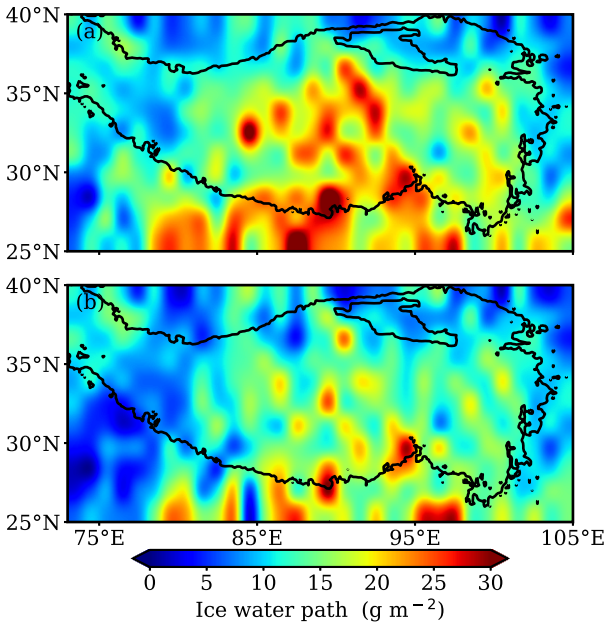

Fig. 9. Distribution of the column total of IWC (a) during DCS + non-DCS events and (b) during non-DCS events in June, July and August. The column total is calculated above 6 km.

onal mean values of IWP between all samples and non-DCS samples. It is apparent that the maximum differences in the latitudinal and meridional mean values are 5.04 and 6.47 g m^{-2}, respectively. These results for the summer IWP distribution imply that DCSs over the Tibetan Plateau and the southern slope have a remarkable impact on the composition of the atmosphere.

5. Conclusions and discussion

Based on the CloudSat CPR 2B_GEOPROF dataset and the Aura MLS Level 2 cloud ice product onboard the A-train constellation of Earth-observing satellites, we analyzed the main detrainment height over the Tibetan Plateau and its southern slope. It was found that the outflow height and horizontal range of DCSs is higher and larger over the central and eastern Tibetan Plateau, the west of the southern slope, and the southeastern edge of the Tibetan Plateau than that over the northwestern Tibetan Plateau. The mean outflow height over the Tibetan Plateau and its southern slope is 12.9 and 13.3 km, respectively, i.e., the mean outflow height over the southern slope is higher than that over the Tibetan Plateau. The anvil heights of DCSs are located at an altitude of about 10–16 km over the Tibetan Plateau and its southern slope. The DCSs with an outflow height of < 13 km and an outflow horizontal range of > 100 km are more frequent at nighttime than during the day. This is because solar radiation produces more convective potential energy and a higher level of neutral buoyancy during daytime. At night, however, the lower temperatures and energy make it difficult for convection to reach a higher outflow height. The DCSs can significantly increase the cloud IWC in the upper troposphere. The cloud IWC increased by 16.8% during DCS events, and the height with the maximum increase is at 178 hPa (about 13 km).

In this study, we characterized the main detrainment height of DCSs by mapping radar echoes and the IWC. However, we only investigated the variations in IWC caused by DCSs, since the IWC is more sensitive to the outflow of DCSs than other trace gases in the atmosphere (e.g., water vapor, methane, CO, SO_2, C_2O_2 and HCN). The distributions of these gases in the UTLS are controlled by many factors, such as the anticyclonic circulation over the Tibetan Plateau, the life cycles of the gases, photochemical processes in the UTLS, and the variation in temperature and relative humidity. How DCSs affect these gases needs further investigation.

Another uncertainty problem comes from the CloudSat datasets. CloudSat only detects at two times in a local area each day, and only operated during the daytime overpass after the power outage in 2011. Thus, the absence of integrated diurnal variation and the sample deviation will influence the final results in terms of the main outflow height. In addition, the study area of the southern slope of the Tibetan Plateau has complex topography and atmospheric circulation, and there are possible differences between the DCSs west and east of the southern slope. We only divided the Tibetan Plateau and the southern slope

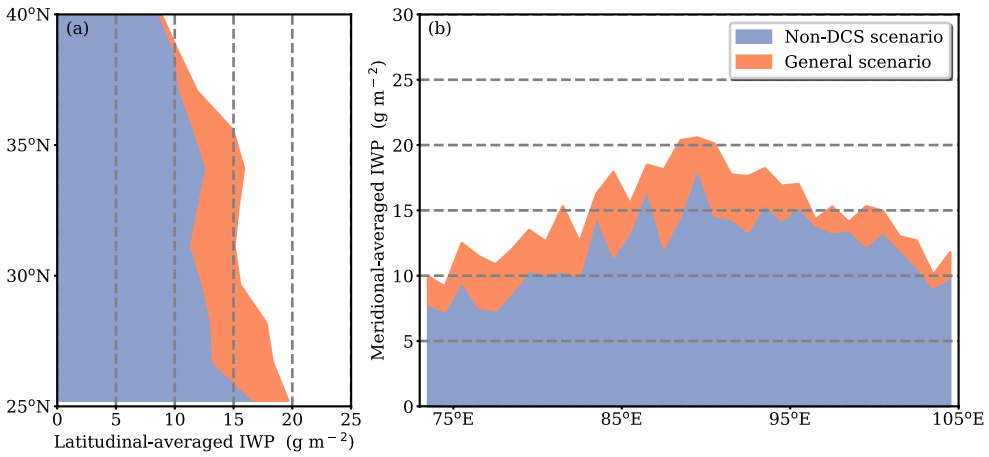

Fig. 10. Changes in column total IWC (a) with latitude and (b) with longitude during DCS + non-DCS events and during non-DCS events.

roughly; it would be worthwhile to discuss the DCSs of the southern slope with a more elaborate subregional structure.

Acknowledgments. This study was supported by the National Key Research and Development Program on Monitoring, Early Warning and Prevention of Major Natural Disasters (Grant No. 2018YFC1506006) and the National Natural Science Foundation of China (Project Nos. 41875108 and 41475037). We are grateful for the online availability of the CloudSat and Aura datasets.

REFERENCES

Alcala, C. M., and A. E. Dessler, 2002: Observations of deep convection in the tropics using the Tropical Rainfall Measuring Mission (TRMM) precipitation radar. *J. Geophys. Res.*, **107**, 4792, https://doi.org/10.1029/2002JD002457.

Andreae, M. O., D. Rosenfeld, P. Artaxo, A. A. Costa, G. P. Frank, K. M. Longo, and M. A. F. Silva-Dias, 2004: Smoking rain clouds over the Amazon. *Science*, **303**, 1337–1342, https://doi.org/10.1126/science.1092779.

Bannister, R. N., A. O'neill, A. R. Gregory, and K. M. Nissen, 2004: The role of the south-east Asian monsoon and other seasonal features in creating the 'tape-recorder' signal in the Unified Model. *Quart. J. Roy. Meteor. Soc.*, **130**, 1531–1554, https://doi.org/10.1256/qj.03.106.

Bedka, K. M., R. Dworak, J. Brunner, and W. Feltz, 2012: Validation of satellite-based objective overshooting cloud-top detection methods using CloudSat cloud profiling radar observations. *Journal of Applied Meteorology and Climatology*, **51**, 1811–1822, https://doi.org/10.1175/JAMC-D-11-0131.1.

Brewer, A. W., 1949: Evidence for a world circulation provided by the measurements of helium and water vapour distribution in the stratosphere. *Quart. J. Roy. Meteor. Soc.*, **75**, 351–363, https://doi.org/10.1002/qj.49707532603.

Cetrone, J., and R. A. Houze Jr., 2009: Anvil clouds of tropical mesoscale convective systems in monsoon regions. *Quart. J. Roy. Meteor. Soc.*, **135**, 305–317, https://doi.org/10.1002/qj.389.

Chen, B., X. D. Xu, S. Yang, and J. C. Bian, 2012: On the characteristics of water vapor transport from atmosphere boundary layer to stratosphere over Tibetan Plateau regions in summer. *Chinese Journal of Geophysics*, **55**, 406–414. (in Chinese)

Chung, E. S., B. J. Sohn, and J. Schmetz, 2008: CloudSat shedding new light on high-reaching tropical deep convection observed with Meteosat. *Geophys. Res. Lett.*, **35**, L02814, https://doi.org/10.1029/2007GL032516.

Corti, T., and Coauthors, 2008: Unprecedented evidence for deep convection hydrating the tropical stratosphere. *Geophys. Res. Lett.*, **35**, L10810, https://doi.org/10.1029/2008GL033641.

Corti, T., B. P. Luo, T. Peter, H. Vömel, and Q. Fu, 2005: Mean radiative energy balance and vertical mass fluxes in the equatorial upper troposphere and lower stratosphere. *Geophys. Res. Lett*, **32**, L06802, https://doi.org/10.1029/2004GL021889.

Danielsen, E. F., 1993: In situ evidence of rapid, vertical, irreversible transport of lower tropospheric air into the lower tropical stratosphere by convective cloud turrets and by larger-scale upwelling in tropical cyclones. *J. Geophys. Res.*, **98**, 8665–8681, https://doi.org/10.1029/92JD02954.

de F. Forster, P. M., and K. P. Shine, 1999: Stratospheric water vapour changes as a possible contributor to observed stratospheric cooling. *Geophys. Res. Lett.*, **26**, 3309–3312, https://doi.org/10.1029/1999GL010487.

de F. Forster, P. M., and K. Shine, 2002: Assessing the climate impact of trends in stratospheric water vapor. *Geophys. Res. Lett.*, **29**, 1086, https://doi.org/10.1029/2001GL013909.

de Rooy, W. C., and A. P. Siebesma, 2008: A simple parameterization for detrainment in shallow cumulus. *Mon. Wea. Rev.*, **136**, 560–576, https://doi.org/10.1175/2007MWR2201.1.

de Rooy, W. C., and A. P. Siebesma, 2010: Analytical expressions for entrainment and detrainment in cumulus convection. *Quart. J. Roy. Meteor. Soc.*, **136**, 1216–1227, https://doi.org/10.1002/qj.640.

Dessler, A. E., 2002: The effect of deep, tropical convection on the tropical tropopause layer. *J. Geophys. Res.*, **107**, 4033, https://doi.org/10.1029/2001JD000511.

Dessler, A. E., and S. C. Sherwood, 2004: Effect of convection on the summertime extratropical lower stratosphere. *J. Geophys. Res.*, **109**, D23301, https://doi.org/10.1029/2004JD005209.

Devasthale, A., and S. Fueglistaler, 2010: A climatological perspective of deep convection penetrating the TTL during the Indian summer monsoon from the AVHRR and MODIS instruments. *Atmospheric Chemistry and Physics*, **10**, 4573–4582, https://doi.org/10.5194/acp-10-4573-2010.

Folkins, I., and R. V. Martin, 2005: The vertical structure of tropical convection and its impact on the budgets of water vapor and ozone. *J. Atmos. Sci.*, **62**, 1560–1573, https://doi.org/10.1175/JAS3407.1.

Folkins, I., M. Loewenstein, J. Podolske, S. J. Oltmans, and M. Proffitt, 1999: A barrier to vertical mixing at 14 km in the tropics: Evidence from ozonesondes and aircraft measurements. *J. Geophys. Res.*, **104**, 22 095–22 102, https://doi.org/10.1029/1999JD900404.

Fu, R., and Coauthors, 2006: Short circuit of water vapor and polluted air to the global stratosphere by convective transport over the Tibetan Plateau. *Proceedings of the National Academy of Sciences of the United States of America*, **103**, 5664–5669, https://doi.org/10.1073/pnas.0601584103.

Fueglistaler, S., A. E. Dessler, T. J. Dunkerton, I. Folkins, Q. Fu, and P. W. Mote, 2009: Tropical tropopause layer. *Rev. Geophys.*, **47**, RG1004, https://doi.org/10.1029/2008RG000267.

Gettelman, A., M. L. Salby, and F. Sassi, 2002: Distribution and influence of convection in the tropical tropopause region. *J. Geophys. Res.*, **107**, 4080, https://doi.org/10.1029/2001JD001048.

Gettelman, A., D. E. Kinnison, T. J. Dunkerton, and G. P. Brasseur, 2004: Impact of monsoon circulations on the upper troposphere and lower stratosphere. *J. Geophys. Res.*, **109**, D22101, https://doi.org/10.1029/2004JD004878.

Hassim, M. E. E., and T. P. Lane, 2010: A model study on the influence of overshooting convection on TTL water vapour. *Atmospheric Chemistry and Physics*, **10**, 9833–9849, https://doi.org/10.5194/acp-10-9833-2010.

Heus, T., and H. J. J. Jonker, 2008: Subsiding shells around shallow cumulus clouds. *J. Atmos. Sci.*, **65**, 1003–1018, https://doi.org/10.1175/2007JAS2322.1.

Highwood, E. J., and B. J. Hoskins, 1998: The tropical tropopause. *Quart. J. Roy. Meteor. Soc.*, **124**, 1579–1604, https://doi.org/10.1002/qj.49712454911.

Holton, J. R., and A. Gettelman, 2001: Horizontal transport and the dehydration of the stratosphere. *Geophys. Res. Lett.*, **28**, 2799–2802, https://doi.org/10.1029/2001GL013148.

Holton, J. R., P. H. Haynes, M. E. McIntyre, A. R. Douglass, R. B. Rood, and L. Pfister, 1995: Stratosphere-troposphere exchange. *Rev. Geophys.*, **33**, 403–439, https://doi.org/10.1029/95RG02097.

Hong, G., G. Heygster, J. Notholt, and S. A. Buehler, 2008: Interannual to diurnal variations in tropical and subtropical deep convective clouds and convective overshooting from seven years of AMSU-B measurements. *J. Climate*, **21**, 4168–4189, https://doi.org/10.1175/2008JCLI1911.1.

Houze, R. A., D. C. Wilton, and B. F. Smull, 2007: Monsoon convection in the Himalayan region as seen by the TRMM Precipitation Radar. *Quart. J. Roy. Meteor. Soc.*, **133**, 1389–1411, https://doi.org/10.1002/qj.106.

Iwasaki, S., T. Shibata, J. Nakamoto, H. Okamoto, H. Ishimoto, and H. Kubota, 2010: Characteristics of deep convection measured by using the A-train constellation. *J. Geophys. Res.*, **115**, D06207, https://doi.org/10.1029/2009JD013000.

Iwasaki, S., T. Shibata, H. Okamoto, H. Ishimoto, and H. Kubota, 2012: Mixtures of stratospheric and overshooting air measured using A-Train sensors. *J. Geophys. Res.*, **117**, D12207, https://doi.org/10.1029/2011JD017402.

Jensen, E. J., L. Pfister, A. S. Ackerman, A. Tabazadeh, and O. B. Toon, 2001: A conceptual model of the dehydration of air due to freeze-drying by optically thin, laminar cirrus rising slowly across the tropical tropopause. *J. Geophys. Res.*, **106**, 17 237–17 252, https://doi.org/10.1029/2000JD900649.

Jensen, E. J., A. S. Ackerman, and J. A. Smith, 2007: Can overshooting convection dehydrate the tropical tropopause layer? *J. Geophys. Res.*, **112**, D11209, https://doi.org/10.1029/2006JD007943.

Khaykin, S., and Coauthors, 2009: Hydration of the lower stratosphere by ice crystal geysers over land convective systems. *Atmospheric Chemistry and Physics*, **9**, 2275–2287, https://doi.org/10.5194/acp-9-2275-2009.

Kingsmill, D. E., and R. A. Houze Jr., 1999: Thermodynamic characteristics of air flowing into and out of precipitating convection over the west Pacific warm pool. *Quart. J. Roy. Meteor. Soc.*, **125**, 1209–1229, https://doi.org/10.1002/qj.1999.>49712555606.

Kirk-Davidoff, D. B., E. J. Hintsa, J. G. Anderson, and D. W. Keith, 1999: The effect of climate change on ozone depletion through changes in stratospheric water vapour. *Nature*, **402**, 399–401, https://doi.org/10.1038/46521.

L'Ecuyer, T. S., and J. H. Jiang, 2011: Touring the atmosphere aboard the A-Train. *AIP Conference Proceedings*, **1401**, 245–256, https://doi.org/10.1063/1.3653856.

Li, Q. B., and Coauthors, 2005: Convective outflow of South Asian pollution: A global CTM simulation compared with EOS MLS observations. *Geophys. Res. Lett.*, **32**, L14826, https://doi.org/10.1029/2005GL022762.

Liu, C. T., E. J. Zipser, and S. W. Nesbitt, 2007: Global distribution of tropical deep convection: Different perspectives from TRMM infrared and radar data. *J. Climate*, **20**, 489–503, https://doi.org/10.1175/JCLI4023.1.

Liu, X. M., E. D. Rivière, V. Marécal, G. Durry, A. Hamdouni, J. Arteta, and S. Khaykin, 2010: Stratospheric water vapour budget and convection overshooting the tropopause: Modelling study from SCOUT-AMMA. *Atmospheric Chemistry and Physics*, **10**, 8267–8286, https://doi.org/10.5194/acp-10-8267-2010.

Livesey, N. J., W. Van Snyder, W. G. Read, and P. A. Wagner, 2006: Retrieval algorithms for the EOS Microwave limb sounder (MLS). *IEEE Trans. Geosci. Remote Sens.*, **44**, 1144–1155, https://doi.org/10.1109/TGRS.2006.872327.

Livesey, N. J., J. A. Logan, M. L. Santee, J. W. Waters, R. M. Doherty, W. G. Read, L. Froidevaux, and J. H. Jiang, 2013: Interrelated variations of O_3, CO and deep convection in the tropical/subtropical upper troposphere observed by the Aura Microwave Limb Sounder (MLS) during 2004–2011. *Atmospheric Chemistry and Physics*, **13**, 579–598, https://doi.org/10.5194/acp-13-579-2013.

Long, Q. C., Q. L. Chen, K. Gui, and Y. Zhang, 2016: A case study of a heavy rain over the southeastern Tibetan plateau. *Atmosphere*, **7**, 118, https://doi.org/10.3390/atmos7090118.

Luo, Y. L., R. H. Zhang, W. M. Qian, Z. Z. Luo, and X. Hu, 2011: Intercomparison of deep convection over the Tibetan Plateau-Asian monsoon region and subtropical North America in boreal summer using CloudSat/CALIPSO data. *J. Climate*, **24**, 2164–2177, https://doi.org/10.1175/2010JCLI4032.1.

Luo, Z. Z., and W. B. Rossow, 2004: Characterizing tropical cirrus life cycle, evolution, and interaction with upper-tropospheric water vapor using Lagrangian trajectory analysis of satellite observations. *J. Climate*, **17**, 4541–4563, https://doi.org/10.1175/3222.1.

Luo, Z. Z., G. Y. Liu, and G. L. Stephens, 2008: CloudSat adding new insight into tropical penetrating convection. *Geophys. Res. Lett.*, **35**, L19819, https://doi.org/10.1029/2008GL035330.

Lü, D. R., and Coauthors, 2009: Frontiers and significance of research on stratospheric processes. *Advances in Earth Science*, **24**, 221–228, https://doi.org/10.3321/j.issn:1001-8166.2009.03.001. (in Chinese)

Mace, G., 2007: Level 2 GEOPROF product process description and interface control document algorithm version 5.3. Colorado State University, 44 pp. [Available online at http://www.cloudsat.cira.colostate.edu/icd/2b-geoprof/2b-geoprof_pdicd_5.3.doc.]

Mapes, B. E., 1993: Gregarious tropical convection. *J. Atmos. Sci.*, **50**, 2026–2037, https://doi.org/10.1175/1520-0469(1993)050<2026:GTC>2.0.CO;2.

Morton, B., G. I. Taylor, and J. S. Turner, 1956: Turbulent gravitational convection from maintained and instantaneous sources. *Proceedings of the Royal Society A*, **234**, 1–23, https://doi.org/10.1098/rspa.1956.0011.

Mote, P. W., and Coauthors, 1996: An atmospheric tape recorder: The imprint of tropical tropopause temperatures on stratospheric water vapor. *J. Geophys. Res.*, **101**, 3989–4006, https://doi.org/10.1029/95JD03422.

Mullendore, G. L., D. R. Durran, and J. R. Holton, 2005: Cross-tropopause tracer transport in midlatitude convection. *J. Geophys. Res.*, **110**, D06113, https://doi.org/10.1029/2004JD005059.

Park, M., W. J. Randel, A. Gettelman, S. T. Massie, and J. H. Jiang, 2007: Transport above the Asian summer monsoon anticyclone inferred from Aura Microwave Limb Sounder tracers. *J. Geophys. Res.*, **112**, D16309, https://doi.org/10.1029/2006JD008294.

Park, M., W. J. Randel, L. K. Emmons, P. F. Bernath, K. A. Walker, and C. D. Boone, 2008: Chemical isolation in the Asian monsoon anticyclone observed in Atmospheric Chemistry Ex-

periment (ACE-FTS) data. *Atmospheric Chemistry and Physics*, **8**, 757–764, https://doi.org/10.5194/acp-8-757-2008.

Park, M., W. J. Randel, L. K. Emmons, and N. J. Livesey, 2009: Transport pathways of carbon monoxide in the Asian summer monsoon diagnosed from Model of Ozone and Related Tracers (MOZART). *J. Geophys. Res.*, **114**, D08303, https://doi.org/10.1029/2008JD010621.

Qie, X. S., X. K. Wu, T. Yuan, J. C. Bian, and D. R. Lu, 2014: Comprehensive pattern of deep convective systems over the Tibetan Plateau-South Asian monsoon region based on TRMM data. *J. Climate*, **27**, 6612–6626, https://doi.org/10.1175/JCLI-D-14-00076.1.

Randel, W. J., and M. Park, 2006: Deep convective influence on the Asian summer monsoon anticyclone and associated tracer variability observed with Atmospheric Infrared Sounder (AIRS). *J. Geophys. Res.*, **111**, D12314, https://doi.org/10.1029/2005JD006490.

Randel, W. J., M. Park, L. Emmons, D. Kinnison, P. Bernath, K. A. Walker, C. Boone, and H. Pumphrey, 2010: Asian monsoon transport of pollution to the stratosphere. *Science*, **328**, 611–613, https://doi.org/10.1126/science.1182274.

Raymond, D. J., and A. M. Blyth, 1986: A stochastic mixing model for nonprecipitating cumulus clouds. *J. Atmos. Sci.*, **43**, 2708–2718, https://doi.org/10.1175/1520-0469(1986)043<2708:ASMMFN>2.0.CO;2.

Romatschke, U., S. Medina, and R. A. Houze Jr., 2010: Regional, seasonal, and diurnal variations of extreme convection in the South Asian region. *J. Climate*, **23**, 419–439, https://doi.org/10.1175/2009JCLI3140.1.

Sassen, K., Z. E. Wang, and D. Liu, 2009: Cirrus clouds and deep convection in the tropics: Insights from CALIPSO and CloudSat. *J. Geophys. Res.*, **114**, D00H06, https://doi.org/10.1029/2009JD011916.

Savtchenko, A., R. Kummerer, P. Smith, A. Gopalan, S. Kempler, and G. Leptoukh, 2008: A-train data depot: Bringing atmospheric measurements together. *IEEE Trans. Geosci. Remote Sens.*, **46**, 2788–2795, https://doi.org/10.1109/TGRS.2008.917600.

Schiller, C., J.-U. Grooß, P. Konopka, F. Plöger, F. H. Silva dos Santos, and N. Spelten, 2009: Hydration and dehydration at the tropical tropopause. *Atmospheric Chemistry and Physics*, **9**, 9647–9660, https://doi.org/10.5194/acp-9-9647-2009.

Sherwood, S. C., 2000: A stratospheric "drain" over the maritime continent. *Geophys. Res. Lett.*, **27**, 677–680, https://doi.org/10.1029/1999GL010868.

Sherwood, S. C., and A. E. Dessler, 2000: On the control of stratospheric humidity. *Geophys. Res. Lett.*, **27**, 2513–2516, https://doi.org/10.1029/2000GL011438.

Sherwood, S. C., and A. E. Dessler, 2003: Convective mixing near the tropical tropopause: Insights from seasonal variations. *J. Atmos. Sci.*, **60**, 2674–2685, https://doi.org/10.1175/1520-0469(2003)060<2674:CMNTTT>2.0.CO;2.

Shi, C. H., W. Y. Cai, and D. Guo, 2017: Composition and thermal structure of the upper troposphere and lower stratosphere in a penetrating mesoscale convective complex determined by satellite observations and model simulations. *Advances in Meteorology*, **2017**, 6404796, https://doi.org/10.1155/2017/6404796.

Solomon, S., K. H. Rosenlof, R. W. Portmann, J. S. Daniel, S. M. Davis, T. J. Sanford, and G.-K. Plattner, 2010: Contributions of stratospheric water vapor to decadal changes in the rate of global warming. *Science*, **327**, 1219–1223, https://doi.org/10.1126/science.1182488.

Solomon, S., J. S. Daniel, R. R. Neely III, J.-P. Vernier, E. G. Dutton, and L. W. Thomason, 2011: The persistently variable "background" stratospheric aerosol layer and global climate change. *Science*, **333**, 866–870, https://doi.org/10.1126/science.1206027.

Squires, P., and J. S. Turner, 1962: An entraining jet model for cumulo-nimbus updraughts. *Tellus*, **14**, 422–434, https://doi.org/10.3402/tellusa.v14i4.9569.

Steiner, M., R. A. Houze Jr., and S. E. Yuter, 1995: Climatological characterization of three-dimensional storm structure from operational radar and rain gauge data. *J. Appl. Meteor.*, **34**, 1978–2007, https://doi.org/10.1175/1520-0450(1995)034<1978:CCOTDS>2.0.CO;2.

Stephens, G. L., and Coauthors, 2002: The CloudSat mission and the A-Train: A new dimension of space-based observations of clouds and precipitation. *Bull. Amer. Meteor. Soc.*, **83**, 1771–1790, https://doi.org/10.1175/BAMS-83-12-1771.

Stephens, G. L., and Coauthors, 2008: CloudSat mission: Performance and early science after the first year of operation. *J. Geophys. Res.*, **113**, D00A18, https://doi.org/10.1029/2008JD009982.

Stohl, A., and Coauthors, 2003: Stratosphere-troposphere exchange: A review, and what we have learned from STACCATO. *J. Geophys. Res.*, **108**, 8516, https://doi.org/10.1029/2002JD002490.

Stommel, H., 1947: Entrainment of air into a cumulus cloud: (Paper presented 27 December 1946 at the Annual Meeting, A M. S., Cambridge, Massachusetts). *J. Meteor.*, **4**, 91–94, https://doi.org/10.1175/1520-0469(1947)004<0091:EOAIAC>2.0.CO;2.

Sun, Y., Q. L. Chen, K. Gui, F. Y. Dong, X. Feng, and Q. C. Long, 2017: Characteristics of water vapor in the UTLS over the Tibetan plateau based on AURA/MLS observations. *Advances in Meteorology*, **2017**, 3504254, https://doi.org/10.1155/2017/3504254.

Takahashi, H., and Z. Z. Luo, 2012: Where is the level of neutral buoyancy for deep convection? *Geophys. Res. Lett.*, **39**, L15809, https://doi.org/10.1029/2012GL052638.

Takahashi, H., and Z. J. Luo, 2014: Characterizing tropical overshooting deep convection from joint analysis of CloudSat and geostationary satellite observations. *J. Geophys. Res.*, **119**, 112–121, https://doi.org/10.1002/2013JD020972.

Tian, W. S., M. Chipperfield, and Q. Huang, 2008: Effects of the Tibetan Plateau on total column ozone distribution. *Tellus B: Chemical and Physical Meteorology*, **60**, 622–635, https://doi.org/10.1111/j.1600-0889.2008.00338.x.

Waters, J. W., and Coauthors, 2006: The earth observing system microwave limb sounder (EOS MLS) on the Aura satellite. *IEEE Trans. Geosci. Remote Sens.*, **44**, 1075–1092, https://doi.org/10.1109/TGRS.2006.873771.

Wright, J. S., A. H. Sobel, and G. A. Schmidt, 2009: Influence of condensate evaporation on water vapor and its stable isotopes in a GCM. *Geophys. Res. Lett.*, **36**, L12804, https://doi.org/10.1029/2009GL038091.

Wu, D. L., and Coauthors, 2008: Validation of the Aura MLS cloud ice water content measurements. *J. Geophys. Res.*, **113**, D15S10, https://doi.org/10.1029/2007JD008931.

Wu, G. X., J. Y. Mao, A. M. Duan, and Q. Zhang, 2004: Recent progress in the study on the impacts of Tibetan Plateau on Asi-

an summer climate. *Acta Meteorologica Sinica*, **62**, 528–540, https://doi.org/10.3321/j.issn:0577-6619.2004.05.002. (in Chinese with English abstract)

Wu, X. K., X. S. Qie, T. Yuan, and J. L. Li, 2016: Meteorological regimes of the most intense convective systems along the southern Himalayan front. *J. Climate*, **29**, 4383–4398, https://doi.org/10.1175/JCLI-D-14-00835.1.

Xu, W. X., 2013: Precipitation and convective characteristics of summer deep convection over East Asia observed by TRMM. *Mon. Wea. Rev.*, **141**, 1577–1592, https://doi.org/10.1175/MWR-D-12-00177.1.

Yuan, J., and R. A. Houze Jr., 2010: Global variability of mesoscale convective system anvil structure from A-Train satellite data. *J. Climate*, **23**, 5864–5888, https://doi.org/10.1175/2010JCLI3671.1.

Yuan, J., R. A. Houze Jr., and A. J. Heymsfield, 2011: Vertical structures of anvil clouds of tropical mesoscale convective systems observed by CloudSat. *J. Atmos. Sci.*, **68**, 1653–1674, https://doi.org/10.1175/2011JAS3687.1.

Zhou, X. J., C. Luo, W. L. Li, and J. E. Shi, 1995: Ozone changes over China and low center over Tibetan Plateau. *Chinese Science Bulletin*, **40**, 1396–1398. (in Chinese)

Zipser, E. J., D. J. Cecil, C. Liu, S. W. Nesbitt, and D. P. Yorty, 2006: Where are the most intense thunderstorms on Earth. *Bulletin of the American Meteorological Society*, **87**, 1057–1072.